Preparation and oxygen sensitivity of a range of noble metal nanoparticles (Ir, Pt, and Au) protected by a series of chalcogen-dodecane ligands (S, Se, and Te)

Vadim Tanygin and Benjamin J. Lear*

The Pennsylvania State University, University Park, PA, 16802, United States of America

E-mail: bul14@psu.edu

Phone: +1 614 814 4625

Abstract

Iridium, platinum, and gold nanoparticles, protected with sulfur, selenium, or tellurium dodecane ligands were synthesized under ambient laboratory conditions. These nine nanoparticles were characterized by thermogravimetric analysis, transmission electron microscopy, and x-ray photoelectron spectroscopy (XPS). XPS was used to determine the degree of oxidation present at the metal-chalcogen interface at the time of synthesis and after one week of aging under ambient laboratory conditions. Upon synthesis, interfaces involving sulfur atoms were found to have no degree of oxidation and to retain this lack of oxidation over the course of one week. In contrast, all interfaces involving tellurium were found to have some degree of oxidation (28%, 77%, and 76% for Ir, Pt, and Au particles, respectively) at the time of synthesis, and this degree of oxidation increased over the course of one week to 38%, 83% and 92% for Ir, Pt, and Au, respectively. For interfaces involving selenium, all interfaces initially lacked any

oxidation and the the iridium and platinum interface was found to be stable over one week. On the other hand, the gold interface oxidized over time, reaching 60% oxidation after one week under ambient laboratory conditions. Thus, our work shows that IrS, IrSe, PtS, PtSe, and AuS provide metal-ligand interfaces that are stable, with respect to oxidation under ambient conditions.

Introduction

For decades, noble-metal nanoparticles (MNPs) have been a mainstay of fundamental and applied materials research. Interest in these systems stems from electronic properties that emerge when metals are confined to the nanoscale, and which can be used to test and refine our fundamental models of solid state physics[1–4] or used as the basis for applications in sensing,[5–7] cancer treatments,[8–10] catalysis,[11–14] and lasers,[15,16] to name a few.

For much of the above effort, controlling the desirable electronic properties of these particles has meant modification of the core—usually through changes to the size and shape.[17–19] However, emerging research on metallic nanoparticles and related atomically precise metal clusters is highlighting the critical role that the metal-ligand interface can play in controlling the electronic behavior of ligand-supported metal cores. For nanoscale systems with such metal-ligand interfaces, Millstone and co-workers have shown that photo-luminescence and magnetism depends on ligands,[20,21] Johnson and co-workers have shown striking changes in absorption properties accompany subtle changes in ligand set,[22–24] Weiss and co-workers have shown that excited state lifetimes and heat capacities can be controlled by ligands,[25] and our own group has shown that the electronic g-factor for metallic electrons depends on the chemical identity of the surfactants.[26–28] Jin and co-workers have shown that even the physical structures of nanoscale metals are impacted by changes to the ligand.[29] Analogous ligand effects arise in calculations performed on small metal clusters by Aikens[30,31] and others[32,33] and can even be seen in bulk gold, where the nature of the molecules used in self-assembled monolayers controls properties such as surface potential of the bulk metal.[34,35]

The link between surface chemistry and electronic behavior suggests that identifying and using ligands that provide chemically stable interfaces will be a critical aspect of nanoscience moving forward. In the absence of such stability, the behaviors of particles will continue to evolve after their synthesis, which nullifies any benefits of careful tuning of the properties via the ligand-metal interface. To the extent that the utility of nanoscale materials depends upon the ability to rationally tune particles for a particular application, it is important to

better understand the chemical stability of metal-ligand interfaces and to identify new stable interfaces that will serve as a scaffold for tuning electronic properties.

At present, one of the best studied metal-ligand interfaces for nanoscale materials is the gold-thiolate interface,[36] which is valued for its ease of synthesis and chemical stability. On the other hand, the latter chalcogens are expected to form stronger bonds with metals and, because of this, potentially exert larger influences over the metal core. Despite this expectation, there is a comparative dearth of experimental investigations into metal-selenolate and metal-tellurolate interfaces at the nanoscale, with the reports on these interfaces often focusing on metal clusters[37] and quantum dots,[38,39] rather than metallic nanoparticles.

Though the stronger expected metal-ligand interactions for Se and Te provide a compelling reason for their use, the representation gap of these interfaces in the literature is not merely an oversight. To a large extent, the lack of representation owes to the fact that so much work on nanoscale metals involves gold, for which the gold-thiolate interface is chemically stable under ambient conditions, while the gold-selenolate[40] and gold-tellurolate[41] interfaces are susceptible to oxidation. Thus, it can be seen that stable interfaces naturally attract a large body of literature, while the additional work required to handle unstable interfaces discourages their use.

It is important to note that the chemical resistance to oxidation of the gold-thiolate interface is not *inherent* to thiols. All chalcogens (including thiols) are susceptible to oxidation. Indeed, disulfides are a well-known and regularly used reagent in organic synthesis.[42] In other words, the oxidative stability of thiols is an *emergent* property of the Au-S interface. This realization motivates us to look for metals other than gold that might lend oxidative stability to interfaces formed between them and the latter chalcogens.

To this end, we undertook a study into the oxidative stability of interfaces between metals and sulfur, selenium and tellurium-based dodecane ligands under ambient laboratory conditions. Given the relatively well-studied nature of the gold-chalcogen interfaces, and the utility of noble metals in nanoscience we began with two other late noble metals, Ir and Pt.

This provided six different nanoparticles: IrSNPs, IrSeNPs, IrTeNPs, PtSNPs, PtSeNPs, and PtTeNPs. In this nomenclature, we give the metal, the chalcogen and then 'NPs' to indicate we are discussing nanoparticles, rather than molecular compounds. In cases were a general chalcogen is referred to, then we use 'E' in place of S, Se, or Te. Given the analogous nature to the gold-chalcogen interface, and the relative abundance of information on that interface, we felt it could be useful to compare the Ir and Pt particles to the gold, and so we prepared gold nanoparticles protected by sulfate, senelolate, and tellurolate dodecane ligands (AuSNPs, AuSeNPs, and AuTeNPs, respectively). Though though we did not find reports of Ir and Pt interfaces involving selenolate or tellurolate ligands in the literature, we found we could adapt common synthetic approaches to produce them. With all nine particles in hand, we used XPS to determine the stability of the interface with respect to oxidation under ambient conditions. We find that, in contrast to gold, both Ir and Pt provide stable interfaces for alkane-selenol ligands, though metal-tellurium interfaces are not stable for any of the metals we examined. Thus, the primary result of this work is the identification of two new stable interfaces that could be used for generating new and stable electronic behaviors of metal nanoparticles.

Experimental

Materials

Tetraoctylammonium bromide (98+%), sodium borohydride (99%, VenPure SF powder), dihydrogen hexachloroplatinate (IV) hexahydrate (99.9%), potassium hexachloroiridate (IV) (min. 39% Ir), sodium thiosulfate (anhydrous, 99%), chloroauric acid trihydrate (99.999%), and tellurium powder (99.5%) were purchased from Alfa Aesar. Dodecanethiol (98+%), dodecylamine (98%), and selenium pellets (<5 mm, 99.99%) were obtained from Sigma-Aldrich. 1-bromododecane (98%) was obtained from Acros Organics. Solvents were obtained from Fisher Chemical. All reagents were used without further purification.

Synthesis

All metal nanoparticles described below may be redispersed in a variety of low-polarity organic solvents, including hexane, toluene, chloroform, and THF. All particles were synthesized and isolated under ambient laboratory conditions. Our laboratory has temperature control, but not humidity control. In general, the lab is kept at $21^\circ \pm 2$C and, during the time the samples were aged, humidity levels fluctuate between 25% and 35%, based upon a wall mounted hygrometer. Unless otherwise noted, samples were exposed to laboratory light, produced by overhead fluorescent bulbs. These lights are turned off when the laboratory is unoccupied, and so each day would include roughly 14 hours of light. Thus, ambient conditions imply exposure to oxygen, humidity, and light. After collection they were stored under a dry nitrogen atmosphere, unless otherwise noted.

Iridium nanoparticles (IrENPs)

Thiolate-protected iridium nanoparticles were synthesized following a literature procedure, with sodium dodecylthiosulfate as the ligand precursor.[43,44]

Selenolate-protected iridium nanoparticles (IrSeNPs) were prepared as follows: Potassium hexachloroiridate (193.2mg, 0.40mmol) was added to a round-bottom flask and dissolved in 30mL Milli-Q ultrapure water. A solution of tetraoctylammonium bromide (1.094g, 2mmol) in 25mL toluene was prepared and added to the stirring hexachloroiridate solution. The mixture was stirred for two hours to ensure complete transfer of hexachloroiridate to the organic phase. The organic phase was collected. Dodecyl diselenide (300mg, 0.60mmol) was added, and the solution stirred before adding a 8mL solution of 1M aqueous sodium borohydride all at once. A color change over several minutes to yellow and then orange indicates the formation of IrSeNPs. The mixture was stirred overnight with the color gradually darkening further. The dark-brown organics were separated, concentrated on a rotary evaporator to a few mL, and 200mL of a 1:1 methanol:ethanol mixture added to precipitate the IrSeNPs. The mixture was stored in a freezer overnight, centrifuged at 10,000rpm for 15 minutes, and

the non-solvent decanted from the pelleted IrSeNPs.

Tellurolate-protected iridium nanoparticles (IrTeNPs) were syntheized following a proceedure similar to that of the selenolate species. However, as dialkyl ditellurides are known to reduce noble metal salts, a reverse-addition protocol was followed. A 10mL solution of 1M tetrabutylammonium borohydride in THF was then added, causing the solution to slowly change from red to yellow-green. This solution was stirred for three minutes, before adding dodecyl ditelluride, which immediately turned the solution a deep red-brown. Finally, 5mL of 1M methanolic sodium borohydride was added, and the solution allowed to stir overnight. The red-brown solution was concentrated on a rotary evaporator to a few mL, and 200mL of a 1:1 methanol:ethanol mixture added to precipitate the IrTeNPs. The mixture was stored in a freezer overnight, centrifuged at 10,000rpm for 15 minutes, and the non-solvent decanted from the pelleted product. The crude product, a mixture of IrTeNPs and a currently uncharacterized orange material, was purified by column chromatography (1:1 hexane:THF eluent), The first band eluted contained the desired IrTeNPs.

Platinum nanoparticles (PtENPs)

All three chalcogenolate-protected particles were synthesized using the same procedure: synthesis of dodecylamine protected particles via a literature procedure,[45] followed by ligand exchange with the target chalcogenolate ligand. Briefly, dihydrogen hexachloroplatinate (0.312g, 0.6mmol) was added to a round-bottom flask and dissolved in 30mL Milli-Q ultrapure water. A solution of tetraoctylammonium bromide (0.984g, 1.8mmol) in 60mL toluene was prepared and added to the stirring dihydrogen hexachloroplatinate acid solution. The mixture was stirred for two hours to ensure complete transfer of hexachloroplatinate to the organic phase.

Dodecylamine (2.44g, 13.2mmol) was then added, and after five minutes of stirring, followed by a dropwise addition of a 20mL solution of aqueous sodium borohydride (0.385g, 10.2mmol). The mixture gradually turned dark brown, and was left to stir for two hours.

The organics were separated and 400mL isopropanol added to precipitate the dodecylamine-protected platinum nanoparticles. The mixture was stored in a freezer overnight, centrifuged at 10,000rpm for 15 minutes, and the non-solvent decanted from the pelleted nanoparticles.

Dodecylamine was replaced with chalcogenolate ligands on the surface through a ligand exchange process. To prepare thiolate-protected nanoparticles, 100mg amine-protected nanoparticles were dispersed in 50mL THF, and 0.347mmol alkanethiol was added. The solution was stirred overnight and precipitated and collected as above to obtain PtSNPs. Using 0.347mmol sodium dodecaneselenolate (prepared by reduction of dodecyl diselenide with a methanolic solution of $NaBH_4$), yields PtSeNPs, and using dodecyl ditelluride yields PtTeNPs. It is important to emphasize that dodecaneselenolate and ditelluride ligands were used for these syntheses.

Gold nanoparticles (AuENPs)

Thiolate,[46] selenolate,[47] and tellurolate-protected gold nanoparticles[41] were synthesized using literature procedures.

Dialkyl dichalcogenides

Dialkyl diselenides[48] and ditellurides[47] were synthesized using literature procedures.

Characterization

Transmission electron microscopy was performed on an FEI Tecnai G20 20 XTWIN LaB6 at an accelerating voltage of 200kV. Samples were prepared by drop-casting dilute nanoparticle dispersions of the NPs onto carbon-coated copper grids (200 mesh, Electron Microscopy Sciences). When feasible, at least 300 particles were counted for each sample.

Thermogravimetric analysis (TGA) measurements were performed using TA Instruments Discovery Series TGA Q5500 coupled with Discovery MS. Samples were held in a platinum

pan and heated from room temperature to 1000 °C at a rate of 20 °C/min under N_2 atmosphere.

XPS experiments were performed using a Physical Electronics VersaProbe II instrument equipped with a monochromatic Al k x-ray source (h = 1,486.7 eV) and a concentric hemispherical analyzer. Samples were drop-cast onto a Si substrate, which was mounted with 3M double sided tape. Charge neutralization was performed using both low energy electrons (less than 5 eV) and argon ions. The binding energy axis was calibrated using sputter cleaned Cu (Cu $2p_{3/2}$ = 932.62 eV, Cu $3p_{3/2}$ = 75.1 eV) and Au foils (Au $4f_{7/2}$ = 83.96 eV). Peaks were charge referenced to CH_x band in the carbon 1s spectra at 284.8 eV. Measurements were made at a takeoff angle of 45 degrees with respect to the sample surface plane. This resulted in a typical sampling depth of 3-6 nm (95 percent of the signal originated from this depth or shallower). Quantification was done using instrumental relative sensitivity factors (RSFs) that account for the x-ray cross section and inelastic mean free path of the electrons.

Results

Synthesis and physical characterization

Synthesis of thiol-protected Ir, Pt, and Au nanoparticles have already been reported,[43–46] and we followed these reported preparations with success. For the latter chalcogens, while we successfully prepared selenolate and tellurolate AuNPs following existing procedures,[41,47] no analogous procedure existed in the literature for either iridium or platinum nanoparticles. In order to maximize the contribution of the surface chemistry, we desired small nanoparticles, which we defined as sub-5nm mean diameter. The most common means of generating such small particles in the literature is through a one- or two-phase synthesis bearing the metal salt and ligands, to which reducing agent is added. Such 'direct' synthesis was found to produce small relatively monodisperse iridium nanoparticles bearing thiolate, selenolate, and tellurolate ligands. Exemplars of the TEMs associated with these particles, as well as

a box and whisker plot of the size distributions can be seen in Figure 1. Histograms of the particles and log-normal fits to the distributions are shown in Figure S1. For all nanoparticle systems, with the exception of the IrSeNPs and IrTeNPs, 300 particles were counted for each histogram. In the case of the IrSeNPs and IrTeNPs, difficulty in acquiring images of sufficient quality for size determination limited us to 148 and 48 particles, respectively. Particularly for the latter, this is very few particles. Thus, the reports of means and standard deviation in size should be judged appropriately. Of course, the increased uncertainty in these values is reflected in the standard errors reported for these values in the SI. However, as the focus of this manuscript was not on size control, but the XPS, this lack of particle counts was not overly concerning to us. The number of particles was sufficient to demonstrate the targeted sub-5nm mean diameter, and justified proceeding with further XPS characterization.

Direct synthesis of PtENPs from hexachloroplatinate salt and dialkyl chalcogenide precursors did not consistently yield small particles with narrow size dispersity; consequently, other routes were explored. Exchange of weakly adsorbed ligands, such as amines, for more strongly bound ligands, such as thiols, is a common method for functionalizing metal nanoparticles while maintaining consistent physical properties of the metal core. We successfully applied this approach to the synthesis of alkanethiolate, alkaneselenolate, and alkanetellurolate protected platinum nanoparticles. Exemplars of the TEMs associated with the final particles, as well as a box and whisker plot of the size distributions can be seen in Figure 1. Histograms of the particles and log-normal fits to the distributions are shown in Figure S1. TEM characterization reveals that platinum nanoparticles initially prepared with dodecylamine ligands retain a similar size, dispersity, and morphology after ligand exchange (Figure S2). Specifically, we find that all three exchanges produce slightly larger particles, with slightly narrower disparities, all with a spheroid shape. XPS verified the presence of chalcogens on the nanoparticle surface after exchange. In the case of PtTeNPs, we also performed elemental mapping to verify that the Pt and Te signals were co-located (Figure S3).

Comparing all of the synthesized particles, the box and whisker plots of Figure 1 show that fairly tight dispersions of particles are generated for both Pt and Ir, with lager dispersions generally associated with the AuTeNPs. From the associated TEMs, it is clear that our syntheses predominantly produce spheroid particles. Though we generally obtain TEM images with excellent contrast, the IrENPs were consistently difficult to obtain clear TEMs, no matter the chalcogen. This difficulty is reflected in the reduced counts for the particle sizes of IrSeNPs and IrTeNPs.

TGA characterization

In addition to determining the size of the particles, we also performed thermogravimetric analysis on both the Ir and Pt particles. Because the Au interfaces have been well characterized[40,41,49] (including TGA), we did not repeat this characterization here. The curves we obtained are shown in Figure S4. For all particles examined, we observed significant mass losses assigned to loss of solvent and ligands. Because the focus is on stability of the interface, as measured by XPS, we do not present a detailed analysis of the TGA. Nevertheless, we can make three comments regarding them here. First, for both metals, the curves for the sulfur ligands were the simplest, reflecting the relative simplicity of this interface (see below). Second, for both metals particles, the tellurium ligands showed multiple high temperature features, indicating that the surface may be more complex than for the sulfur interface. Finally, we notice that, in general, the smaller particles experience larger percent mass losses, consistent with the fact that the smaller the particles the larger percent composition is due to the ligands. Thus, the TGA curves we obtain are in *qualitative* agreement with the remainder of our findings.

XPS characterization

We used XPS to determine the degree of oxidation of the chalcogenide-metal interfaces. Specifically, we focused on the oxidation of the chalcogen, using the signals associated with ionization from the 2p, 3d, and 4d orbitals of the S, Se, and Te atoms, respectively. In the case of Te, signals involving both the 3d and 4d orbitals can provide usable data, and sometimes the transition involving the 3d orbital discussed in the literature;[41,50] however, we decided to focus on the highest energy subshell of the chosen ℓ value. This choice was made to provide more similarity between final states, when compared to using identical orbitals for elements in different periods. Specifically, the 3d orbital for Te is much lower energy than the 3d orbital for Se, which can cause larger differences in the final state and depth of sampling of reported on by XPS, than when comparing transitions involving the 3d orbital in Se and 4d orbital in Te. Finally, we note that, though we could observe XPS signals associated with ionization from the metal atoms, these signals arise from atoms at both the surface and bulk, making isolation of the interface difficult. For this reason, we felt the chalcogens provided a more selective probe of the interface, and we focus on their signals.

To determine the stability of the interface with respect to oxidation, we characterized both 'as-prepared' samples and 'aged' samples, which had been exposed to ambient conditions for one week. For the as-synthesized samples, the particles were isolated, immediately resuspended in dichloromethane, and dropped-cast on a Si substrate. These samples were then stored under a dry nitrogen atmosphere in a glovebox until their analysis. Thus, the as-synthesized samples do not imply oxygen-free conditions; rather, they report on the conditions of the particles, when freshly prepared under the ambient conditions described in the experimental section. The focus of the paper is on if these particles continue to evolve post-synthesis.

After acquiring XPS on the as-synthesized samples, the samples were then left under ambient laboratory conditions (as described in the experimental section) for 1 week, after which XPS was again acquired. Thus, the same samples that provided the as-synthesized

spectra, also provided the aged spectra.

Figure 2 shows the XPS spectra for regions including signals associated with S 2p, Se 3d, and Te 4d of the IrENPs, PtENPs, and AuENPs. In this figure, the open circles are the collected data. The data was fit to a linear combination of Lorentzian profiles and Tourgaard background,[51] the result of this fit is shown as the solid black line. To aid in interpretation, the individual Lorentzian profiles are shown as the shaded regions. Lorentzians that are associated with the chalcogen at the interface are shaded in either red (oxidized) or blue (unoxidized). Lorentzians shaded in gray come from other contributions, such as metal orbitals, or chalcogens that are not assigned to the metal-ligand interface. All assignments of the Lorentzians are made based upon the position of the Lorentzian maximum (Table 1), as detailed below for each chalcogen. Finally, we note that, for ease of comparison between samples, the data shown in Figure 2 have had the Tourgaard background subtracted. Raw spectra are shown in Figure S6.

When fitting and interpreting the data in Figure 2 is important to remember that the S, Se, and Te signals involve transitions from 2p, 3d, and 4d orbitals respectively. Because these orbitals have $\ell \neq 0$, each give rise to a doublet of peaks, associated with two different spin states. For signals involving the p-orbitals, the individual peaks are associated with $p_{3/2}$ and $p_{1/2}$ states, while for those involving from d-orbitals, they are associated with $d_{5/2}$ and $d_{3/2}$ states. The ratio of intensities within each doublet is given by theory to be 1:2 for $p_{1/2}$:$p_{3/2}$ and 2:3 for $d_{3/2}$:$d_{5/2}$. These intensity ratios within each double are enforced during the fitting.

The energy separation between band maxima within a doublet is expected to be the same for each species, as is the widths of the individual Lorentzian profiles. Thus, for each spectrum, the separation between maxima and the profile widths for the doublets are allowed to vary by a small amount ($\pm 1\%$). Because the magnitude of the splitting between peaks is an adjustable parameter, we present the position the signals from both spin-states. Though it is common to report the position of a single peak, we give the position of both peaks of

the doublet so that the validity of the model's (with respect to the adjustable parameters) can be judged. The equations used for the fitting and a discussion of the fitting approach is detailed in the SI.

For this report, the parameter of most interest obtained from the the fitting of the XPS spectra is the area of the doublets. The relative areas of the doublets for the oxidized (red profiles) and non-oxidized (blue profiles) species can be used to estimate the degree of oxidation at the interface. The fractional composition of he oxidized species at the interface (f_{EOx}) is giving in Figure 2 for each sample. It is important to realize that this analysis ignores the contribution from the grey profiles, which we do not assign to species specific to the interface. The specific assignment of the grey bands and the results of fitting are discussed next, grouped by chalcogen.

sulfur

Though XPS of thiols on all three metals are already known in the literature,[40,41,44,52] we are unaware of studies that specifically address changes to the XPS upon aging of the particles. Even though the thiol interface is expected to be stable, we include these result in order to establish the method that we apply to the other chalcogens. The existence of prior XPS studies greatly simplifies the assignments of the peaks that we observe for the thiolate-protected nanoparticles. The signals we report on involve the S 2p orbital. The prior work on gold nanoparticles reported values of 164.2 eV ($2p_{1/2}$) and 162.9 eV ($2p_{3/2}$) for the sulfur bound to gold.[40] In the prior reports on Ir and Pt nanoparticles, the doublet was not explicitly considered, and peak position was given by the maximum of the overall XPS band. A binding energy of ca. 162 eV was reported for both platinum and iridium. Given the separation between the doublet maximums (ca. 1-2 eV) and the widths expected for the individual Lorentzians, the overall profile maximum reported in the prior studies is expected to be a good approximation for the more intense of the Lorentzian profile ($p_{3/2}$) of the doublet.

Examination of Table 1 shows the values we extract for the signals involving the 2p are in good agreement with the prior reported values for thiolate-protected nanoparticles.[40] It is worth noting here that, while the binding energies we obtain for the thiolate on the gold nanoparticles are larger than observed for thiolates on Au(111) surfaces,[53–55] they are in agreement with prior work on nanoparticles.[40] This likely reflects the fact that the chemical environment found at the interfaces of the nanoparticle is different from that found at uniform Au(111) surfaces.

It is also worth noting the relative complexity for the Ir particles. Decomposition of this spectrum into Lorentzians requires three doublets (Figure 2). The doublet at the lowest binding energy is assigned to the metal-chalcogen interface. The other two doublets are assigned to thiosulfate remaining from the synthesis. Three facts allow us to make these assignments with confidence. First, the lowest energy doublet is in the best agreement with the expected position for sulfur at metal interfaces. Second, the 'extra' features align closely with literature values for thiosulfate (ca. 166–168 eV), which was used in our synthesis.[44] Finally, the prior report on thiolate-protected iridium nanoparticles also reported the presence of thiosulfate bands in the XPS, yielding an overall profile similar to the one we observe.[44]

Examination of Figure 2 will show that the XPS spectra in the S 2p region of all three particles remains essentially unchanged upon aging. Specifically, we observe no evidence for the emergence of oxidized thiols at the thiol-metal interface, which should present as new features at higher binding energy. Of course, oxidized sulfur signals do appear for the iridium samples, but we again assign them as thiosulfate remaining from the synthesis.[43,44] Thus, all three interfaces appear to be stable with respect to oxidation on the timescale of weeks.

It is worth noting here that our analysis only speaks to the *stability* of the interface, rather than to the species present. Even for the extremely well characterized gold-thiolate interface, the interface is complex and multiple species are possibly present at the interface.[36] The same is expected to hold true for the selenolate and tellurolate interfaces discussed below. For the iridium and platinum particles, the interfaces are less-well characterized than for gold and,

given the relative reactivity of these metals, it is reasonable to expect them to be even more complex. However, despite this complexity, the XPS measurements do provide insight into the oxidative stability of the interface that is present.

selenium

The XPS of Se on Ir and Pt is unreported. However there is a prior XPS study of Se on AuSeNPs,[40] which assigned the $3d_{5/2}$ to a feature with binding energy of 55.2 eV, and did not assign the associated $3d_{3/2}$ contribution. Our fitting of the AuSeNPs XPS allows assignment of both members of the 3d doublet to 55.9 eV ($3d_{5/2}$) and 56.8 eV ($3d_{3/2}$). In addition, we include a doublet assigned as involving the 5p orbital of Au, shown in grey in Figure 2. The appropriateness of including this doublet, and the validity of its assignment, is testified to by the XPS of pure bulk gold, which shows a clear band that can be fit to a doublet arising from a transition involving a p-orbital (Figure S5). We do note that the binding energy we obtain for the Se bound to gold is larger than prior reports for nanoparticles[40] or on Au(111) surfaces.[56] At this time, we do not have an explanation for our larger observed binding energy. As a reminder, in the case of the AuSNPs discussed above, the thiolates attached to nanoparticles give different values from those attached to Au(111) surfaces and so we might expect that the values found for AuSeNPs would differ from those arising from Au(111) films. Given the paucity of XPS studies on AuSeNPs, it is hard to know if our deviation from the single prior report on selenolate-protected gold nanoparticles is spurious or not. The establishment of a larger body of work will be needed to make this judgement.

Even in light of questions concerning the precise expected value of the binding energy, our results allow comment on the degree of oxidation at the metal-selenolate interface, which is the focus of this report. For the as-synthesized particles, a single Se 3d doublet and the Au 5p doublet yields satisfactory agreement with the experimental spectrum for the as-synthesized AuSeNPs. Thus, we do not find evidence for oxidized selenium at the time that the AuSeNPs are oxidized.

Just as the binding energy for S 2p was similar across all three metals (see above), we expect that the the position of the Se 3d doublets for Ir and Pt particles will be similar to those for the Au particles. This reasoning allows us to assign the pairs of peaks at 55.1 eV ($d_{5/2}$) and 56.3 eV ($d_{3/2}$) for the as-synthesized Ir and 55.0 eV ($d_{5/2}$) and 56.0 eV ($d_{3/2}$) for the as-synthesized Pt. For the Ir samples, the spectrum is satisfactorily fit using just this single doublet, without the need for oxidized species. However, for Pt, there is again contribution from the metal, in this case, a doublet associated with the Pt 5p orbital. Inclusion of this contribution produces satisfactory fits of the spectrum, without the need for contributions from oxidized Se.

The above analysis suggests that no significant oxidized selenium exists for the as-synthesized particles of all three metals. We also find that aging of the particles produces little change to the XPS spectra for Ir and Pt, indicating that these interfaces are resistant to oxidation on the timescale of weeks.

However, we do find that aging of the particles leads the emergence of a new feature at higher binding energy for the AuSeNPs. This new feature is much narrower than the contribution from Au 5p, and so we do not assign this as a new Au 5p signal. Instead, fitting of the spectrum for AuSeNPs requires the addition of a new doublet that has similar spacing and width as the unoxidized Se 3d signal. This doublet has features at at 58.1 eV eV ($d_{5/2}$) and 58.9 eV ($d_{5/2}$) and is assigned to oxidized Se. The possible chemical nature of the oxidized Se is addressed in the discussion section.

tellurium

As was the case for Se, prior reports of XPS of our particles exist only for AuTeNPs,[41] which reported a spectrum with the 4d doublet at 43.54 eV ($4d_{5/2}$) and 44.93 eV ($4d_{3/2}$) and assigned these signals to oxidized Te. In this prior report, a shoulder was present at lower binding energy, but was not commented on. We observe a similarly shaped spectrum for the *aged* AuTeNPs (Figure 2). However, in the spectrum for the as-synthesized sample, the

lower binding energy feature is much more prominent, to the point that it provides a resolved maximum. The overall spectrum is then fit by addition of a second $4d_{5/2,3/2}$ doublet at lower energy. Thus, we conclude that the as-synthesized AuTeNPs contains both unoxidized and oxidized species of Te, with a high energy (oxidized) doublet at 43.0 eV ($4d_{5/2}$) and 44.3 eV ($4d_{3/2}$) and a low binding energy (unoxidized) doublet at 40.4 eV ($4d_{5/2}$) and 41.8 eV ($4d_{3/2}$). These positions are also consistent with those found for an Te-based ligand bound to Au(111).[57]

The assignments of the Te spectrum for the Ir and Pt particles follow directly from those for the AuNPs. Indeed, we find that adequate fitting of the Te 4d region for both the as-synthesized and the aged samples of all three metals requires two doublets. The locations of all Lorentzians are given in Table 1. The doublet at large binding energies we assign to oxidized Te and doublet at smaller banding energies we assign to unoxidized Te. In other words, we always observe the presence of both oxidized and unoxidized Te, no matter the identity of the metal.

Though oxidized Te is present for the as-synthesized samples of our nanoparticles, the degree of oxidation continues to evolve over time, with all samples also showing an increase in the relative proportion of oxidized Te upon aging. We also note that within the as synthesized and aged series of samples, the degree of oxidation follows the order Ir $<$ Pt $\leq$ Au. The possible identity of the oxidized species is considered in the discussion section.

Discussion

The motivation for this study was to understand the oxidative stability of the interfaces present for Ir, Pt, and Au nanoparticles bearing S, Se, and Te-based ligands. The reason for exploring the chalcogenides was their relative abundance in the nanoparticle literature, their known susceptability to oxidation, and the emergent oxidative resistance for the Au-S interface. Though other binding motifs are known for metals, such as amines,[58] isocyanides,[59]

alkynes,[60] and carbenes,[61] these binding groups are not as susceptible to oxidation as the chalcogenides, and so emergent resistance to oxidation would not be required for stability of the interface.

To begin with, we note that the results shown in Figure 2 demonstrate that interfaces based upon S and Se can be prepared under ambient conditions without oxidized species present at the interface for all three metals. Though we do observed oxidized species present in the case of the IrSNPs, we again note that prior work assigns this as residual thiosulfate, not expected to be present at the as-synthesized interface. Thus, in the case of S and Se-based interfaces, keeping particles under inert conditions would presumably preserve the non-oxidized nature of the interface. In contrast, all particles bearing Te-based ligands contained oxidized species, as synthesized. As a reminder, all nine particles examined here were produced under the ambient laboratory conditions described in the experimental section, which included exposure to oxygen, moisture, and light. Thus, in order to produce non-oxidized species, it would likely be necessary to synthesize the tellurolate-bearing particles under inert conditions.

The results shown in Figure 2 clearly show that interfaces based upon S are stable to oxidation for all three metals, on the timescale of weeks. This result is expected, and a large reason why thiols are so widely used as metal binding groups for the organic surfactants used in the synthesis of metallic nanoparticles.

Our results also show that Se provides a stable interface for both Ir and Pt. Se is not a commonly used binding group in the literature of gold surface science, either for nanoparticles or for self-assembled monolayers on bulk gold. In part, this is due to the difficulty in preparing oxidatively stable interfaces, and so much of the work on Au-Se interfaces has been conducted in the context measurements performed under vacuum. Our work shows that, if Se interfaces are of interest, Ir and Pt provide more stable interfaces under ambient conditions.

The final result, in regards to oxidative stability, is that tellurium does not provide a stable interface for any of the metals examined. Over the course of a week, we see statistically

significant oxidation of this interface for all three metals. In addition, for all three metals, both oxidized and unoxidized signals remain. However, for gold, it seems likely that the interface may eventually completely oxidize, after which point it would become stable towards further oxidation.

The changes in oxidation of the Se and Te interfaces raises the question as to the chemical identity of the oxidized species. Though we emphasize that the focus of the this study was on *whether* the interface changed, rather than what it changed to, we can speculate some regarding the possible identity of the oxidized Se and Te species.

For Se, it is likely that the oxidized species present is SeO_2. The nature of the gold-selenolate interface has been studied, and Se(IV) species are the predominant oxidation products found.[62] Furthermore, the chemical shift of the oxidized species corresponds closely with the shift known for pure SeO_2.[63] Although the shifts do not match perfectly, the difference is small enough to attribute to the interaction with the underlying gold surface of the nanoparticle. As neither the Ir nor the Pt interface showed oxidation, we do not need to comment on the nature of the oxidized species for those metals.

The identity of the tellurium species on each metal is more uncertain. As neither IrTeNPs nor PtTeNPs have been reported prior to this report, there is no prior information available to guide this discussion. For AuTeNP interface, the one study on AuTeNPs claimed that the ligands are adsorbed predominantly as telluroxide (R-(Te=O)-Au) based on the Te:O atomic ratio and observed chemical shift in binding energy of the Te electrons upon oxidation.[41] A comparable ratio and shift (for the oxidized component) was observed for the AuNPs synthesized in our work, but only after aging; aging shifts both components by +0.50eV compared to freshly prepared AuNPs. Thus, we feel it is likely that we have the same species present at our AuTeNPs. Given the similarity between the spectra for the IrTeNP, PtTeNP, and AuTeNP interfaces, it seems likely that the same oxidized Te species are present in all three cases, although more work is needed to clearly establish the exact speciation present at the metal-tellurium interfaces.

Finally, though we did obtain mass spectra associated with the TGA measurements, we were unable to find any conclusive evidence for speciation at the surface. This is likely due to the mass cutoff for the instrument, which occurs at m/z=201. Thus, the suspected oxidized tellurium and selenium species would only be present for fragments containing less than 3 carbons or less than 7 carbons for Te and Se, respectively. However, we find no evidence for fragments of this size. The absence of these fragments, however, should not be taken as conclusive evidence for absence of the suspected species, as it could simply be that the longer chain carbon does not yield these fragments in appreciable amounts, under our instrumental conditions. Thus, the identity of the surface species must remain inconclusive. Nevertheless, no matter the exact chemical identities, the results here demonstrate that care will be needed if one is to characterize or exploit the properties of Ir, Pt, or Au particles protected by Te-based ligands. On the other hand, both Ir and Pt provide substrates on which the influence of S and Se ligands can be examined and designed, without concern over the oxidative evolution of the interface during analysis and use.

Conclusions

We have synthesized and characterized the oxidative stability under ambient laboratory conditions over the timescale of weeks for nine metal nanoparticles: Ir, Pt, and Au particles protected with dodecane-chalcogen ligands (chalcogen = S, Se, and Te). Of these, four particles (IrSeNPs, PtSeNPs, IrTeNPs, and PtTeNPs) are new. For all metals we examined, the sulfur binding group provides an interface that is oxidatively stable over the course of a week. For particles bearing selenium-based ligands, all particles initially do not posses oxidized species. Both the IrSeNPs and PtTeNPs remain unoxidized over the course of a week, while oxidized selenium appears for the AuSeNPs. When employing tellurium as the ligand binding group, oxidation is present at the time of synthesis for all three metals, and the degree of oxidation at the interface continues to increase over the course of a week of

aging. This study reveals that IrSeNPs and PtSeNPs provide new interfaces that can be used to explore the dependence of nanoparticle properties of changes in chalcogen binding group, and to provide new electronic properties without worry over the stability of the interface.

Acknowledgement

The authors acknowledge the NSF (CHE 16-09572) for financial support of this work. The authors also thank Dr. Jeff Shallenberger for many helpful discussions regarding the interpretation of XPS spectra.

Supporting Information Available

Histograms of particle diameters and log normal fits to these distributions, EDS map for PtTe particles, TGA curves, XPS of bare gold, raw XPS for the particles, and a discussion of fitting procedures for XPS.

This material is available free of charge via the Internet at `http://pubs.acs.org/`.

References

(1) Halperin, W. P. Quantum Size Effects in Metal Particles. *Review of Modern Physics* **1986**, *58*, 533–606.

(2) Halas, N.; Lal, S.; Chang, W. S.; Link, S.; Nordlander, P. Plasmons in Stronly Coupled Metallic Nanostuctures. *Chemical Reviews* **2011**, *111*, 3913–3961.

(3) Zengin, G.; Johansson, G.; Johansson, P.; Antosiewics, T. J.; Kall, M.; Schgai, T. Approaching the strong coupling limit in single plasmonic nanorods interacting with J-aggregates. *Scientific Reports* **2013**, *3*, 3074.

(4) Ealias, A. M.; Saravankumar, M. P. A review on the classification, characterization, synthesis of nanoparticles and their application. *IOP Conference Series:* **2017**, *263*, 032019.

(5) Stawart, M. E.; Anderton, C. R.; Thompson, L. B.; Maria, J.; Gray, A. K.; Rogers, J. A.; Nuzzo, R. G. Nanostructured Plasmonic Sensors. *Chemical Reviews* **2008**, *108*, 494–521.

(6) Willets, K. A.; Duyne, R. P. V. Localized Surface Plasmon Resonance Spectroscopy and Sensing. *Annual Review of Physical Chemistry* **2007**, *58*, 267–297.

(7) Anker, J. N.; Hall, W. P.; Lyandres, O.; Shah, N. C.; Zhao, J.; Duyne, R. P. V. Biosensing with plasmonic nanosensors. *Nature Materials* **2008**, *7*, 442–453.

(8) Bardhan, I.; Lal, S.; Joshi, A.; Halas, N. J. Theranostic Nanoschells: From Probe Design to Imaging and Treatment of Cancer. *Accounts of Chemical Research* **2011**, *44*, 936–946.

(9) Huan, X.; Jain, P. K.; El-Sayed, I. H.; El-Sayed, M. A. Plasmonic photothermal therapy (PPTT) using gold nanoparticles. *Lasers in Medical Science* **2007**, *23*, 217–228.

(10) Dreaden, E. C.; Alkilany, A. M.; Huang, X.; Murphy, C. J.; El-Sayed, M. A. The golden age: gold nanoparticles for biomedicine. *Chemical Society Reviews* **2012**, *41*, 2740–2279.

(11) Zhang, Y.; Cui, X.; SHi, F.; Deng, Y. Nano-Gold Catalysis in Fine Chemical Synthesis. *Chemical Reviews* **2012**, *112*, 2467–2505.

(12) Haruta, M.; Tsubota, S.; Kobayashi, T.; Kageyama, H.; Genet, M.; Delmon, B. Low-Temperature oxidation of CO over Gold Supported on TiO_2, α-Fe_2O_3, and Co_3O_4. *Journal of Catalysis* **1993**, *144*, 175–192.

(13) Saavedra, J.; Doan, H. A.; Pursell, C. J.; Grabow, L. C.; Chandler, B. D. The critical role of water at the gold-titania interface in catalytic CO oxidation. *Science* **2008**, *345*, 1599–1602.

(14) Clavero, C. Plasmon-induced hot-electron generation at nanoparticle/metal-oxide interfaces for photovoltaic and photocatalytic devices. *Nature Photonics* **2014**, *8*, 95–103.

(15) Oulton, R. F.; Orger, V. J.; Zentgraf, T.; Ma, R. M.; Gladden, C.; Dai, L.; Bartal, G.; Zhang, X. Plasmonic lasers at deep subwavelength scale. *Nature* **2009**, *461*, 629–632.

(16) Sidiropoulos, T. P. . H.; Roder, R.; Geburt, S.; Hess, O.; Maier, S. A.; Ronning, C.; Oulton, R. F. Ultrafast plasmonic nanowire lasers near the surface plasmon frequency. *Nature Physics* **2014**, *10*, 870–876.

(17) Jung, L. S.; Campbell, C. T.; Chinowsky, T. M.; Mar, M. N.; Yee, S. S. Quantitative Interpretation of the Response of Surface Plasmon Resonance Sensors to Adsorbed Films. *Langmuir* **1998**, *14*, 5636–5648.

(18) Chen, H.; Kou, X.; Yang, Z.; Ni, W.; Wang, J. Shape- and Size-Dependent Refractive Index Sensitivity of Gold Nanoparticles. *Langmuir* **2008**, *24*, 5233–5237.

(19) Link, S.; El-Sayed, M. Size and Temperature Dependence of the Plasmon Absorption of Colloidal Gold Nanoparticles. *The Journal of Physical Chemistry B* **1999**, *103*, 4212–4217.

(20) Andolina, C. M.; Dewar, A. C.; Smith, A. M.; Marbella, L. E.; Hartmann, M. J.; Millstone, J. E. Photoluminescent GoldCopper Nanoparticle Alloys with Composition-Tunable Near-Infrared Emission. *Journal of the American Chemical Society* **2013**, *135*, 5266–5269.

(21) Hartmann, M. J.; Millstone, J. E.; Hkkinen, H. Ligand Mediated Evolution of Size

Dependent Magnetism in Cobalt Nanoclusters. *Physical Chemistry Chemical Physics* **2018**, *20*, 4563.

(22) Cirri, A.; Hernndez, H. M.; Kmiotek, C.; Johnson, C. J. Systematically Tuning the Electronic Structure of Gold Nanoclusters through Ligand Derivatization. *Angewandte Chemie, International Edition* **2019**, *58*, 13818–13822.

(23) Schilter, D. Gold called to action. *Nature Reviews Chemistry* **2019**, *3*, 512.

(24) Cirri, A.; Hernández, H. M.; Johnson, C. J. Hydride, chloride, and bromide show similar electronic effects in the $Au_9(PPh_3)_8^{3+}$ nanocluster. *Chemical Communications* **2020**, *56*, 1283–1285.

(25) Peterson, M. D.; Cass, L. C.; Harris, R.; Edme, K.; Sung, K.; Weiss, E. A. The Role of Ligands in Determining the Exciton Relaxation Dynamics in Semiconductor Quantum Dots. *Annual Review of Physical Chemistry* **2014**, *65*, 317–339.

(26) Cirri, A.; Silakov, A.; Lear, B. J. Ligand Control over the Electronic Properties within the Metallic Core of Gold Nanoparticles. *Angewandte Chemie* **2015**, *254*, 11750–11753.

(27) Cirri, A.; Silakov, A.; Jensen, L.; Lear, B. J. Probing ligand-induced modulation of metallic states in small gold nanoparticles using conduction electron spin resonance. *Physical Chemistry Chemical Physics* **2016**, *18*, 25443–25451.

(28) Cirri, A.; Silakov, A.; Jensen, L.; Lear, B. J. Chain Length and Solvent Control over the Electronic Properties of Alkanethiolate-Protected Gold Nanoparticles at the Molecule-to-Metal Transition. *Journal of the American Chemical Society* **2016**, *138*, 15987–15993.

(29) Higaki, T.; Chenjie Zeng, Y. C.; Hussaina, E.; Jin, R. Controlling the Crystalline Phases (FCC, HCP and BCC) of Thiolate-Protected Gold Nanoclusters by Ligand-Based Strategies. *Crystal Engineering Communications* **2016**, *18*, 6979–6986.

(30) Weerawardene, K. L. D. M.; Aikens, C. M. Effect of aliphatic versus aromatic ligands on the structure and optical absorption of $Au_{20}(SR)_{16}$. *The Journal of Physical Chemistry C* **2016**, *120*, 8354–8363.

(31) Weerawardene, K. L. D. M.; Aikens, C. M. Origin of photoluminesence of $Ag_{25}(SR)_{18}^{-}$ nanoparticles: Ligand and doping effect. *Journal of Physical Chemistry C* **2018**, *122*, 2440–2447.

(32) Nikitina, N. A.; Pichugina, D. A.; Kuzmenko, N. E. Quantum chemical assessment of the ligand effect on the properties and structure of protected gold clusters. *Russian Journal of Physical Chemistry A* **2017**, *91*, 1507–1512.

(33) Zhong, J.; Tang, X.; Tang, J.; Su, J.; Pei, Y. Density Functional Theory Studies on Structure, Ligand Exchange, and Optical Properties of Ligand-Protected Gold Nanoclusters: Thiolate versus Selenolate. *The Journal of Physical Chemistry C* **2015**, *119*, 9205–9214.

(34) Serino, A. C.; Anderson, M. E.; saley, L. M. A.; Dziedzic, R. M.; Mills, H.; Heidenreich, L. K.; Spokoyny, A. M.; Weiss, P. S. Work function control of germanium through carborane-carboxylic acid surface passivation. *ACS Applied Materials and Interfaces* **2017**, *9*, 34592.

(35) Evans, S. D.; Ulman, A. Surface potential studies of alkyl-thiol monolayers adsorbed on gold. *Chemical Physics Letters* **1990**, *170*, 462–466.

(36) H Häkkinen, The gold-sulfur interface at the nanoscale. *Nature Chemistry* **2012**, *4*, 443–455.

(37) Kang, X.; Zhu, M. Metal Nanoclusters Stabilized by Selenol Ligands. *Small* **2019**, *15*, 1902703.

(38) Buckley, J. J.; Couderc, E.; Greaney, M. J.; Munteanu, J.; Riche, C. T.; Bradforth, S. E.; Brutchey, R. L. Chalcogenol LIgand Toolbox for CdSe Nanocrystals and Their Influence on Exciton Relaxation Pathways. *ACS Nano* **2014**, *8*, 2512–2521.

(39) Hughes, B. K.; Ruddy, D. A.; Blackburn, J. L.; Smith, D. K.; Bergren, M. R.; Nozik, A. J.; Johnson, J. J.; Beard, M. C. Control of PbSe Quantum Dot Surface Chemistry and Photophysics Using an Alkylselenide Ligand. *ACS Nano* **2012**, *6*, 5498–5506.

(40) Yee, C. K.; Ulman, A.; Ruiz, J. D.; Parikh, A.; White, H.; Rafailovich, M. Alkyl Selenide- and Alkyl Thiolate-Functionalized Gold Nanoparticles: Chain Packing and Bond Nature. *Langmuir* **2003**, *22*, 9450–9458.

(41) Li, Y.; Silverton, L. C.; Haasch, R.; Tong, Y. Y. Alkanetelluroxide-Protected Gold Nanoparticles. *Langmuir* **2008**, *24*, 7048–7053.

(42) Wuts, P. G. M.; Greene, T. W. *Greene's protective groups in organic synthesis*, 4th ed.; 10; Wiley: New York, 2006; pp 462,692.

(43) Isaacs, S. R.; Cutler, E. C.; Park, J. S.; Lee, T. R.; Shon, Y. S. Synthesis of tetraoctylammonium-protected gold nanoparticles with improved stability. *Langmuir* **2005**, *21*, 5689–5692.

(44) Gavia, D. J.; Do, Y.; Gu, J.; Shon, Y.-S. Mechanistic Insights into the Formation of Dodecanethiolate-Stabilized Magnetic Iridium Nanoparticles: Thiosulfate vs Thiol Ligands. *The Journal of Physical Chemistry C* **2014**, *118*, 14548–14554.

(45) Wikander, K.; Petit, C.; Holmberg, K.; Pileni, M.-P. Size Control and Growth Process of Alkylamine-Stabilized Platinum Nanocrystals: A Comparison between the Phase Transfer and Reverse Micelles Methods. *Langmuir* **2006**, *22*, 4863–4868.

(46) Brust, M.; Walker, M.; Bethell, D.; Schiffrin, D. J.; Whyman, R. Synthesis of thiol-

derivatised gold nanoparticles in a two-phase LiquidLiquid system. *Journal of the Chemical Society, Chemical Communications* **1994**, 801–802.

(47) Li, Y.; Zaluzhna, O.; Xu, B.; Gao, Y.; Modest, J. M.; Tong, Y. J. Mechanistic Insights into the BrustSchiffrin Two-Phase Synthesis of Organo-chalcogenate-Protected Metal Nanoparticles. *Journal of the American Chemical Society* **2011**, *133*, 2092–2095.

(48) Deacon, M. L.; Zelakiewicz, B. S.; Tong, Y. Y. A Fast and Convenient One-Pot Synthesis of Dioctyldiselenide at Ambient Temperature and Atmosphere. *Synlett* **2005**, *2005*, 1618–1620.

(49) Woehrle, G. H.; Brown, L. O.; Hutchison, J. E. Thiol-Functionalized, 1.5-nm Gold Nanoparticles through Ligand Exchange Reactions: Scope and Mechanism of Ligand Exchange. *Journal of the American Chemical Society* **2005**, *127*, 2172–2183.

(50) Bahl, M. K.; Watson, R. L.; Irgolic, K. J. Xray photoemission studies of tellurium and some of its compounds. *The Journal of Chemical Physics* **1977**, *66*, 5526–5535.

(51) Hesse, R.; Denecke, R. Improved Tougaard background calculation by introduction of fittable parameters for the inelastic electron scattering cross-section in the peak fit of photoelectron spectra with UNIFIT 2011. *Surface and Interface Analysis* **2010**, *43*, 1514–1526.

(52) Castro, E. G.; Salvatierra, R. V.; Schreiner, W. H.; Oliveira, M. M.; Zarbin, A. J. G. Dodecanethiol-Stabilized Platinum Nanoparticles Obtained by a Two-Phase Method: Synthesis, Characterization, Mechanism of Formation, and Electrocatalytic Properties. *Chemistry of Materials* **2010**, *22*, 360–370.

(53) Shaporenko, A.; Ulman, A.; Terfort, A.; Zharnikov, M. Self-Assembled Monolayers of Alkaneselenolates on (111) Gold and Silver. *The Journal of Physical Chemistry B* **2005**, *109*, 3898–3906.

(54) Bain, C. D.; Biebuyck, H. A.; Whitesides, G. M. COmparison of Self-Assembled Monolayers on Gold: Coadsorption of Thiols and Disulfides. *Langmuir* **1989**, *5*, 723.

(55) Fabianowski, W.; Coyle, L. C.; Weber, B. A.; Granata, R. D.; Castner, D. G.; Sadownik, A.; Regen, S. L. Spontaneous assembly of phosphatidylcholine monolayers via chemisorption onto gold. *Langmuir* **1989**, *5*, 35–41.

(56) Fser, M. A.; Sauter, E.; Zharnikov, M.; Terfort, A. Synergism in Bond Strength Modulation Opens an Alternative Concept for Protective Groups in Surface Chemistry. *The Journal of Physical Chemistry C* **2018**, *122*, 28839–28845.

(57) Weidner, T.; Shaporenko, A.; Mller, J.; Hltig, M.; Terfort, A.; Zharnikov, M. Self-Assembled Monolayers of Aromatic Tellurides on (111)-Oriented Gold and Silver Substrates. *The Journal of Physical Chemistry C* **2007**, *111*, 11627–11635.

(58) Yang, G.; Chang, W.; Jr., D. T. H. A convenient phase transfer protocol to functionalize gold nanoparticles with short alkylamine ligands. *Journal of Colloid and Interface Science* **2015**, *460*, 164–172.

(59) Joo, S. W.; Kim, W. J.; Yun, W. S.; Choi, I. S. Binding of aromatic isocyanides on gold nanoparticle surfaces investigated by surface-enhanced Raman scattering. *Applied Spectroscopy* **2004**, *58*, 218–223.

(60) Zhang, S.; Chandra, K. L.; Gorman, C. B. Self-Assembled Monolayers of Terminal Alkynes on Gold. *Journal of the American Chemical Society* **2007**, *129*, 4876–4877.

(61) Bridonneau, N.; Hippolyte, L.; Mercier, D.; Portehault, D.; Murr, M. D.-E.; Marcus, P.; Fensterbank, L.; Chanac, C.; Ribot, F. N-Heterocyclic carbene-stabilized gold nanoparticles with tunable sizes. *Dalton Transactions* **2018**, *47*, 6850–6859.

(62) Romashov, L. V.; Ananikov, V. P. Self-Assembled Selenium Monolayers: From Nan-

otechnology to Materials Science and Adaptive Catalysis. *Chemistry A European Journal* **2013**, *19*, 17640–17660.

(63) Wagner, C.; Riggs, W. M.; Davis, L.; Moulder, J. *Handbook of X-Ray Photoelectron Spectroscopy*; Perkin-Elmer Corporation, 1979; p 92.

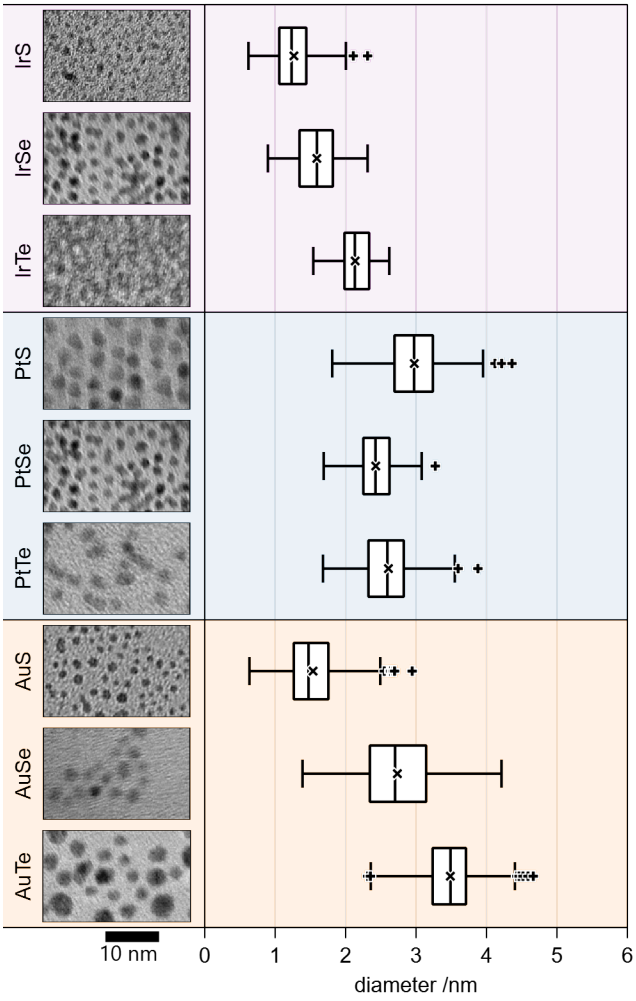

Figure 1: TEM exemplars and box and whisker plots of the distribution of diameters obtained from TEM for the final products of our syntheses. All TEMs share the same scale bar, shown at the bottom of the figure. For the box and whisker plots, the median size is given by the line in the middle of the box, while the mean is indicated by the '×'. The box contains the inner quartile of diameters, the whiskers mark 1.5 times the inner quartile, and any particles outlying this range are marked by the '+' symbols.

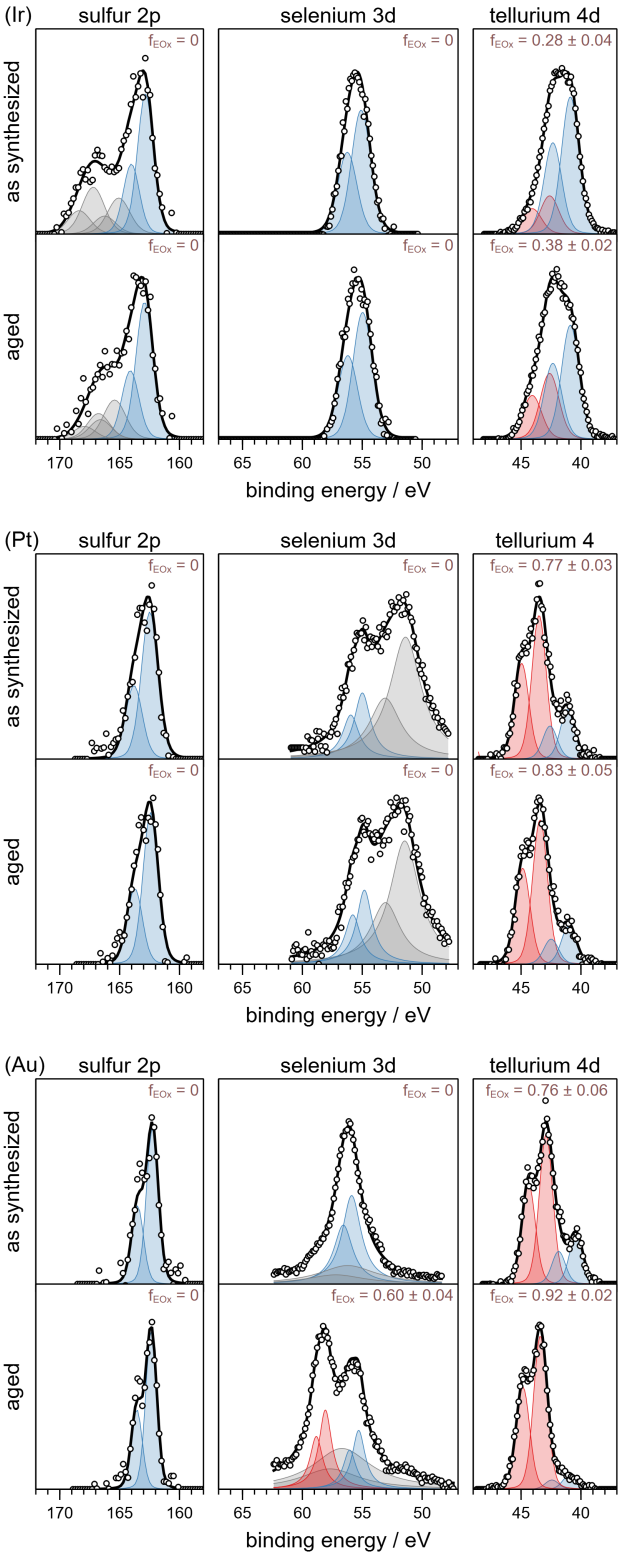

Figure 2: Background corrected XPS spectra of the MNPs before and after aging. The uncorrected spectra can be found in the SI. For each spectrum, the open circles indicate the experimental data and the solid black line indicates the fit to this data. Fits are comprised of several pairs of Lorentzian profiles. Profiles assigned to the chalcogen-metal interface are colored either blue (non-oxidized chalcogen) or red (oxidized chalcogen). The relative area of these Lorentzian profiles are used to determine the fraction of the surface that is oxidized, which is given in the top right corner of each plot. Lorentzian profiles not assigned to the chalcogen-metal interface are shown in grey for the IrS, PtSe, and AuSe systems. These are assigned to thiosulfate S 2p , Pt 5p , and Au 5p, respectively.

Table 1: Positions of the Lorentzians components of the fits to the experimental spectrum. Given are are the positions of the profiles associated with the chalcogenides assigned to the metal-ligand interface. These are the Lorentzians shown as either blue (non-oxidized) or red (oxidized) in Figure 2. The error in the maxima were ±0.1 eV or less, for each band

species	**condition**	binding energy / eV	binding energy / eV
		S $3p_{1/2}$	S $3p_{3/2}$
IrS	fresh	164.1	162.9
IrS	aged	164.1	162.9
PtS	fresh	163.4	162.1
PtS	aged	163.5	162.1
AuS	fresh	163.3	162.2
AuS	aged	163.4	162.3
		Se $3d_{3/2}$	Se $3d_{5/2}$
IrSe	fresh	56.3	55.1
IrSe	aged	56.2	55.0
PtSe	fresh	56.0	55.0
PtSe	aged	55.8	54.8
AuSe	fresh	56.8	55.9
AuSe	aged	56.1	55.3
$AuSeO_x$	fresh	—	—
$AuSeO_x$	aged	58.9	58.1
		Te $4d_{3/2}$	Te $4d_{5/2}$
IrTe	fresh	42.3	40.9
IrTe	aged	42.3	40.9
PtTe	fresh	42.6	41.1
PtTe	aged	42.5	41.0
AuTe	fresh	41.8	40.4
AuTe	aged	42.4	41.0
$IrTeO_x$	fresh	44.1	42.5
$IrTeO_x$	aged	44.1	42.7
$PtTeO_x$	fresh	44.9	43.5
$PtTeO_x$	aged	44.9	44.9
$AuTeO_x$	fresh	44.3	43.0
$AuTeO_x$	aged	44.8	43.4

Graphical TOC Entry